27

UPTEC 92 029E

FEB 1992

AN ESTIMATION OF MICRO VERTEX TRACK ERRORS IN DELPHI AT LEP USING THREE PRONG TAU EVENTS

ANNA DELIN

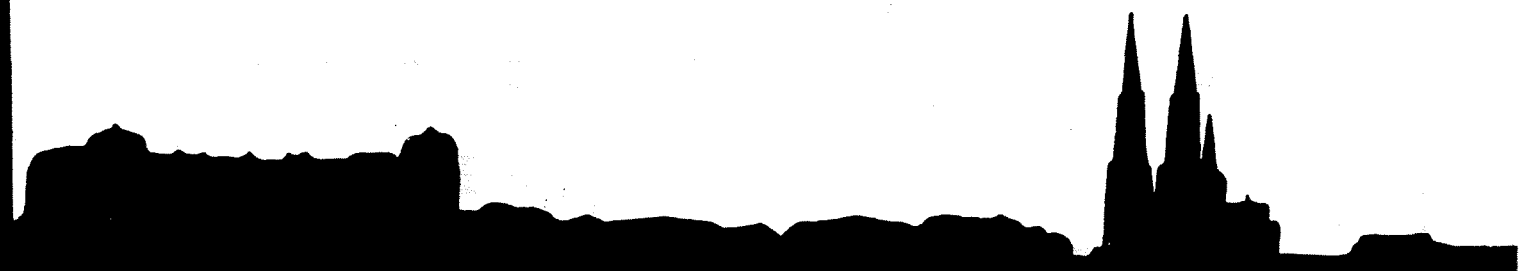

TEKNIKUM

INSTITUTE OF TECHNOLOGY

UPPSALA UNIVERSITY

ISSN 0346-8887

UPPSALA UNIVERSITET
TEKNISKA HÖGSKOLAN
TEKNIKUM
Institutionen för teknologi

UPPSALA UNIVERSITY
Department of Technology

UPTEC 92029E

Date of issue
February 1992

Project name

Sponsoring organization

Author(s)
Delin, Anna

Title (Swedish)

Title (English)

An Estimation of Micro Vertex Track Errors in DELPHI at LEP Using Three Prong Tau Events

Abstract

The average error in the track impact parameter at the collision vertex is found to be 56 μm. A determination of the partial contributions to this error from multiple Coulomb scattering and from alignment errors, respectively, yields (62$\pm$14) μm (p = momentum in GeV/c) and 24.4$\pm$ 2.0 μm. These results are found to be in accordance with expectations. The result for the error arising from alignment uncertainties also agrees with earlier measurements using muons.

Keywords / Indexing

Security

Language
English

Supplementary bibliographical information

Pages
44

Classification

ISSN 0346-8887

ISBN

Postal address
Box 534
S-751 21 Uppsala
Sweden

Visiting address
Villavägen 4
Uppsala

Phone
+46-18-18 25 00
direct no:
+46-18-18 30 08
(librarian)

Fax
+46-18-15 50 95

Telex
76143
UPTEC-S

This thesis has been presented to the Faculty of the Department of Technology, Uppsala University, in partial fulfillment of the requirements for the degree Master of Science in Engineering Physics.

An Estimation of Micro Vertex Track Errors in DELPHI at LEP Using Three Prong Tau Events

Anna Delin, University of Uppsala

February 13, 1992

Abstract

The average error in the track impact parameter at the collision vertex is found to be 56 μm. A determination of the partial contributions to this error from multiple Coulomb scattering and from alignment errors, respectively, yields (62$\pm$14) μm (p = momentum in GeV/c) and 24.4$\pm$ 2.0 μm. These results are found to be in accordance with expectations. The result for the error arising from alignment uncertainties also agrees with earlier measurements using muons.

Contents

1 Introduction

Reconstruction of particle tracks is an important part of the analysis in most particle physics experiments. This report presents two different ways of determining how accurately a particle track can be measured.

We begin with a short summary of the basic concepts of elementary particle physics.

1.1 Particle physics at LEP

Particle physics deals basically with the study of the basic constituents of matter and of the interactions between them [1]. The current picture is recapitulated in a theory called the Standard Model. At the present time, it states that all matter is made up of the six quarks and the six leptons listed in table 1. These particles are called fermions because they have half integer spin. Ordinary matter is made up from the members of the first column or generation. The two additional generations have been observed in particle physics experiments and in cosmic rays. The tau neutrino and the top quark have yet to be observed experimentally, although there are good theoretical evidence for their existence. The quarks seem to exist only in bound states containing two or three quarks. These bound states are called hadrons.

The fermions interact by exchange of fundamental bosons—particles with integer spin—which are the carriers of four distinct types of fundamental interaction. Three of these are listed in table 2. The fourth one, gravity, is left out since it has negligible effect compared with the others within the scope of particle physics.

Experimental research in the field of elementary particle physics require giant particle accelerators in order to acheive the high energies needed in the reactions. In Europe, the largest accelerators are situated at CERN—the european centre for particle physics. The most recent accelerator built at CERN is LEP, the Large Electron and Positron collider. It is currently in its first phase, operating at the Z^0 resonance energy 91.2 GeV. Four experiments are active at LEP: ALEPH, DELPHI, L3, and OPAL. The results presented in this paper are valid for the DELPHI-experiment and the data it collected during 1991.

Table 1: The elementary fermions. For each particle given there is an associated anti-particle. The quarks are named up, down, charm, strange, top and bottom. There are three charged leptons — the electron, muon and tau — and three neutral leptons: the electron, muon and tau neutrinos.

Quarks

charge			
$\begin{pmatrix} +\frac{2}{3} \\ -\frac{1}{3} \end{pmatrix}$	$\begin{pmatrix} u \\ d \end{pmatrix}$	$\begin{pmatrix} c \\ s \end{pmatrix}$	$\begin{pmatrix} t \\ b \end{pmatrix}$

Leptons

charge			
$\begin{pmatrix} 0 \\ -1 \end{pmatrix}$	$\begin{pmatrix} \nu_e \\ e \end{pmatrix}$	$\begin{pmatrix} \nu_\mu \\ \mu \end{pmatrix}$	$\begin{pmatrix} \nu_\tau \\ \tau \end{pmatrix}$

Table 2: Three of the fundamental interactions.

Interaction	Particle	Range (cm)
Electromagnetic	γ	∞
Weak	W^+, W^-, Z^0	10^{-16}
Strong	g	10^{-13}

1.2 Objective

The large statistics attainable at LEP allow precision measurements and tests of the Standard Model [2]. One aspect of this — relevant for this report — is the study of the charm and bottom quarks, often referred to as the heavy quarks. Hadrons containing heavy quarks have very short lifetimes, they typically decay only a few millimeters away from the production point where they were created. The point of decay is named secondary vertex, see figure 1. In order to investigate these hadrons, their decays are reconstructed from the tracks registered in the detector. Here, high precision tracking and good knowledge of the errors are essential.

This report concerns the positional errors on secondary vertices close to the production point and errors on the track impact parameter in the same region.

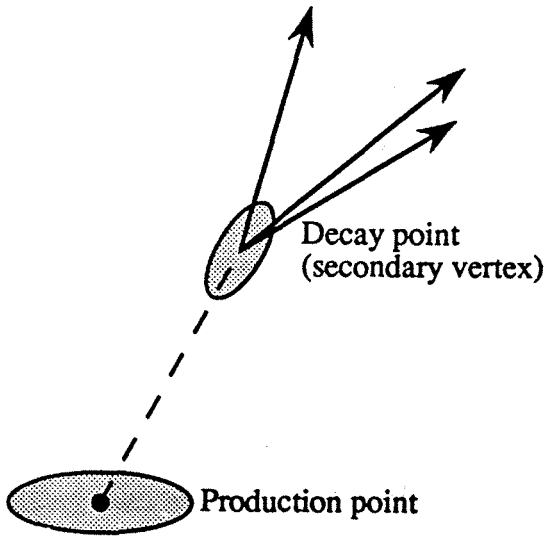

Figure 1: A particle is produced at the production point and decays at the secondary vertex.

The errors on tracks, statistical and systematic, have several sources, the most important being multiple scattering, alignment, detector resolution and energy loss. In this paper an estimation is made of the contribution to the impact parameter error from three of the above named sources: multiple scattering, alignment and detector resolution.

The heaviest charged lepton — the tau — has a lifetime of the same order as hadrons containing heavy quarks. Further, its decays are easy to recognize

in a detector, which makes it useful for various kinds of measurements. These two characteristics makes it very suitable for our purposes. In this analysis we will use a sample of $e^+e^- \rightarrow Z^0 \rightarrow \tau^+\tau^-$ events, where one of the produced taus decay into three charged tracks.

1.3 A word on conventions

All variables I and ϵ stand for random variables or one measurement of the corresponding random variable. The coordinate system used throughout is such that the z-axis is parallel to the beam. The $r\phi$-plane is perpendicular to the z-axis and θ is the polar angle in a sperical coordinate system.

2 The DELPHI Experiment

DELPHI, (DEtector with Lepton Photon and Hadron Identification), has been operating at LEP since 1989. It is designed as a general purpose detector with powerful particle identification especially in mind. Its specific attributes are the ring imagining Cherenkov counters, RICH, and the three-layer micro-Vertex Detector, VD.

2.1 Physics goals

An important goal in DELPHI is to tag heavy quarks. This can be done by reconstructing secondary vertices resulting from hadronic decays of heavy quarks or looking at impact parameters of leptons produced in semileptonic decays. As mentioned, a primary B-meson travels typically about two millimeters before decaying. Hadrons containing charm quarks have even shorter tracks. The short flight distance makes the decay vertex hard to distinguish from the primary vertex. A good particle identification combined with high precision on impact parameters and reconstructed vertices is thus crucial for the tagging of heavy quarks [3].

2.2 The detector

Here the general layout of of the DELPHI detector will be described briefly. A more complete description is given in [4]. The VD is described in somewhat more detail, since the results presented later are closely related to the performance of this detector.

A perspective view of DELPHI is shown in figure 2. It consists of a cylindrical section, the barrel, and two end-caps.

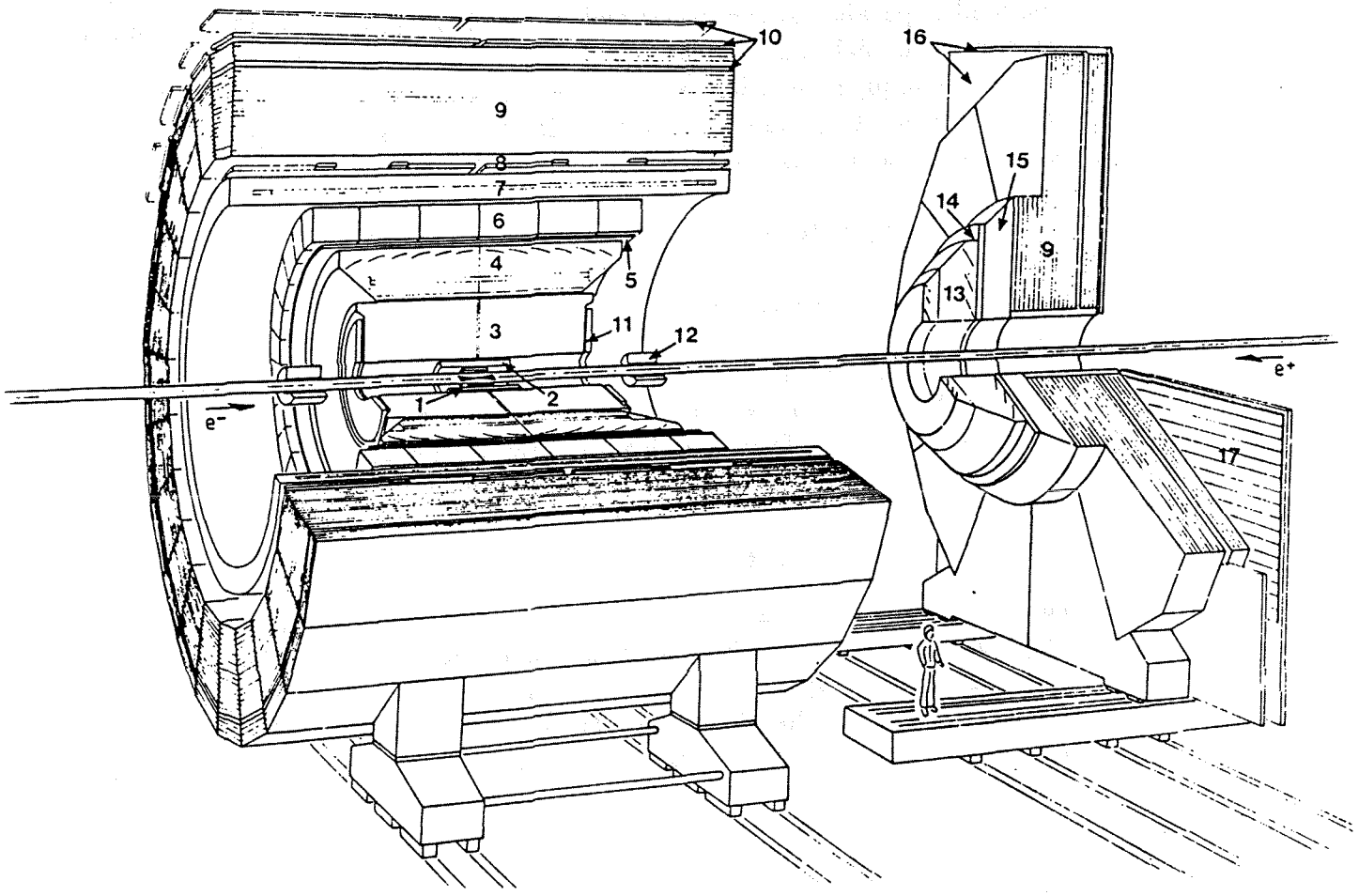

1	micro-vertex detector	10	barrel muon chambers
2	inner detector	11	forward chamber A
3	time projection chamber	12	small angle tagger (SAT)
4	barrel ring imaging Cherenkov counter (RICH)	13	forward RICH
5	outer detector	14	forward chamber B
6	high density projection chamber (HPC)	15	forward electromagnetic calorimeter
7	superconducting solenoid	16	forward muon chambers
8	time of flight counters (TOF)	17	forward scintillator hodoscope
9	hadron calorimeter		

Figure 2: Perspective view of the DELPHI detector. The very small angle tagger (VSAT) falls outside the view.

The magnetic field of 1.2 T is produced by a superconducting solenoid. The field is parallel to the z-axis and is very homogenous. A 45 GeV muon traversing this field has a maximum track radius of about 145 m.

The beam pipe has a diameter of 112 mm and its wall is 1.4 mm thick. It is made from beryllium in order to minimize the effects of multiple scattering. A 1 GeV/c particle is scattered typically 0.7 mrad by the material in the beampipe.

The tracking detectors in DELPHI are the micro-Vertex Detector (VD), the Inner Detector, ID, the Time Projection Chamber, TPC, and the Outer Detector, OD. Of these, the VD has the best resolution in $r\phi$ and the TPC the best resolution in z. The TPC is also the principal pattern recognition device in DELPHI; track reconstruction starts from its information.

The RICH, a velocity measuring device, sits between the TPC and the OD. The combined information from the tracking detectors and the RICH is used for particle identification.

2.2.1 The micro-vertex detector

The VD, shown in figure 3, consists of three concentric cylindrical silicon layers and covers 2π in the azimuthal angle and 43° to 137° in the polar angle. The closer layer has a mean radius of 63 mm, the inner 88 mm and the outer 108 mm. The silicon plaquettes cover each 15° in $r\phi$ with overlaps between sectors. Accurate alignment of the detector is made possible by these overlap regions.

The n-doped silicon crystals are 280 μm thick. One face is covered with 5 μm p-doped diode strips and aluminium contacts. The distance between the strips, the pitch, is 25 μm with every other strip read out [5].

The principle for particle detection is illustrated in figure 4. Connecting the strips to negative voltage depletes the n-doped silicon of free charge carriers and produces a electric field in the crystal. A high-energy particle traversing the detector will produce a narrow tube of electron-hole pairs around its path. Under the influence of the electric field, the electrons drift towards the ground plane and the holes towards the diode strips where they are collected. The signals so produced are read out by charge-sensitive amplifiers. The hit position is found by weighting together signals from adjacent read out strips. In beam tests resolutions better than 10 μm have been obtained [6].

At the moment the VD gives only information in the $r\phi$-plane but a double-sided detector, which would give also the z-coordinates of the hits, is under developement.

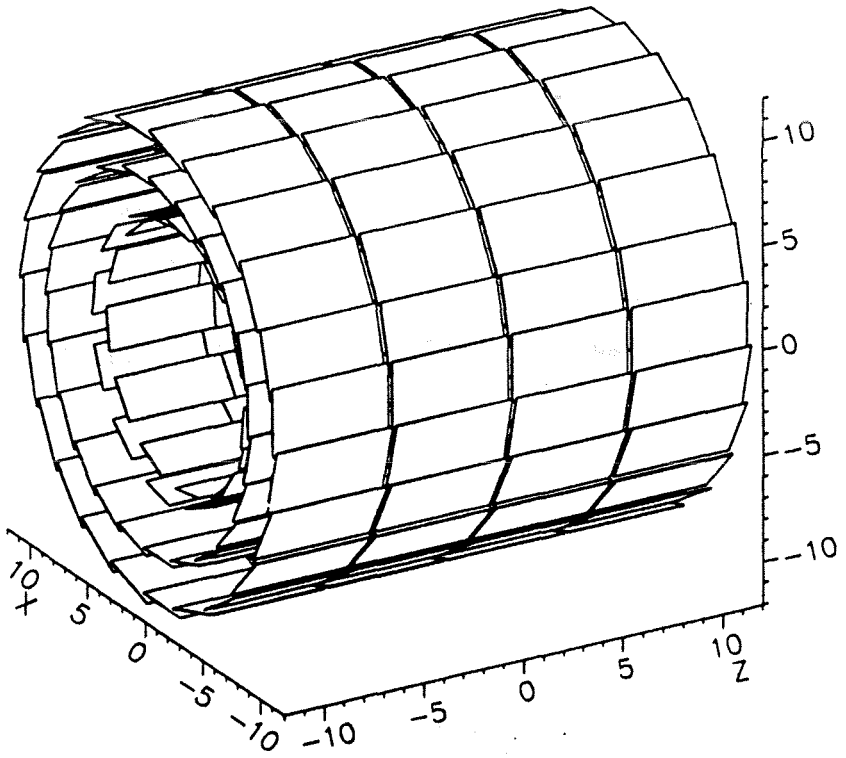

Figure 3: The three-layer VD.

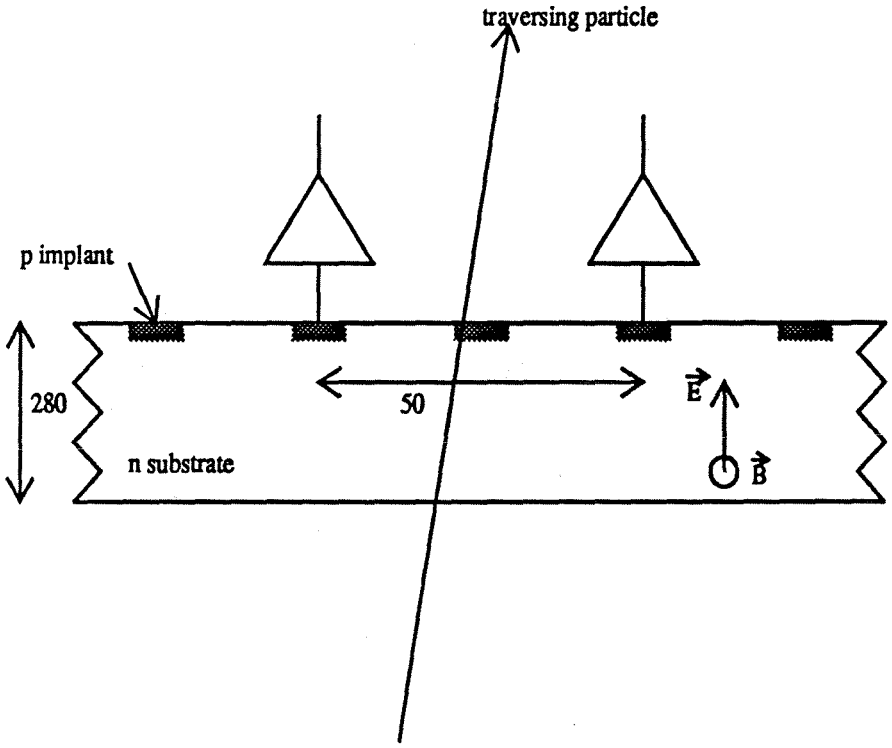

Figure 4: Plaquette with traversing particle. [7]

3 Tau Decays

Since tau decays play an important part in this analysis, a short review of the tau lepton and its decay modes is in order.

The tau lepton was discovered in 1975 at the e^+e^- collider SPEAR. Since then, a thorough investigation of its properties has been made by a number of experiments [8]. Their results all indicate that the τ lepton interacts in the same way as the other two known charged leptons, the electron and the muon. In the framework of the Standard Model the τ is placed in a third lepton doublet together with its associated neutrino ν_τ. Figure 5 shows the first order diagram for τ-pair production in a e^+e^--collider.

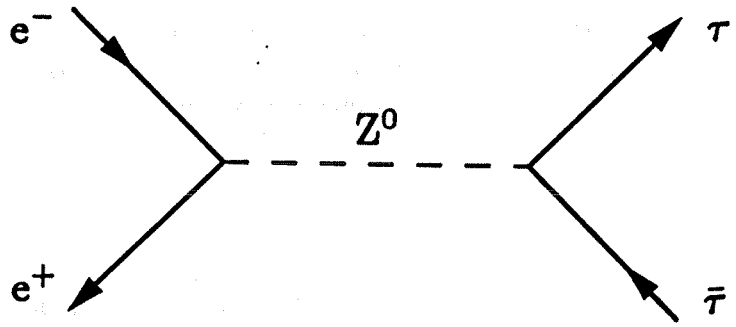

Figure 5: First order Feynman diagram for τ-pair production in e^+e^--annihilation at the Z^0-resonance.

However, because of its relatively large mass, the tau behaves very differently from the electron and the muon. Several hadrons are lighter than the tau, making semihadronic tau decay possible, see figure 6. Such a decay has the form of a very narrow jet consisting of only a few particles; a pencil jet.

The momentum spectrum of the hadronic tau decay products is relatively wide, as shown in figure 7. Since low momentum tracks are more sensitive to multiple scattering, this opens the possibility of using tau decays to estimate the effect of multiple scattering.

In order analyse tau decays, it is convenient to group the decays into different topologies depending on the signal registered in the detector. Only

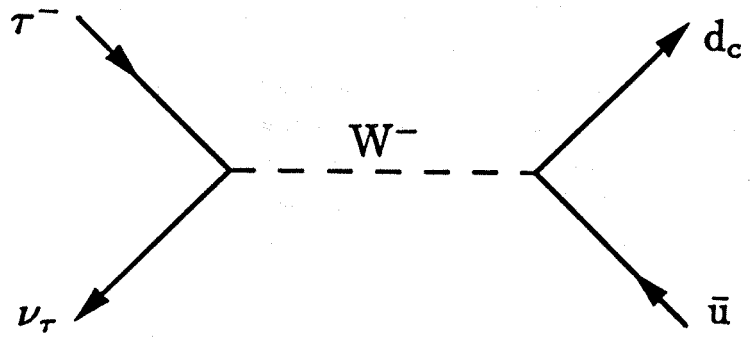

Figure 6: First order diagram for the semihadronic τ decay. The tau decays weakly into the light quarks d_C and u. d_c is a mixed state of the d and s quarks. This state is produced in weak decay whereas the quark states in table 1 are produced in strong decay.

charged particles produce visible tracks, and therefore the decays are divided into different groups depending on the number of charged tracks. A decay into one charged particle and an arbitrary number of neutrals is called a one-prong decay whereas a decay into three charged particles (and additional neutrals) is a three-prong decay. Five-prong decays also exist, but they are much more rare than the other two topologies.

The branching ratios (BR) are given in table 3. We see that the one-prong decays are by far the most frequent ones.

Tables 4 and 5 show in more detail the different channels for one-prong and three-prong decay respectively. A specific state always implies its charge conjugate as well. It should be noted that the decay commonly has an intermediate state in form of a short lived resonance. The decay $\tau \rightarrow \nu_\tau \pi^- \pi^0$ is dominated by the ρ meson and in the three-prong case the ω and the A_1 resonances are often formed.

The channels containing strange particles (mostly kaons) are not given here. They all have branching ratios in the order of one percent or less.

Table 3: Measurements of the topological branching ratios of tau decays [8]. The numbers quoted are world averages.

decay	BR (%)
one-prong	86.5 ± 0.3
three-prong	13.4 ± 0.3
five-prong	0.14 ± 0.04

Table 4: Branching ratios for the most important one-prong channels. [8]

decay	BR (%)
$\tau \rightarrow \nu_\tau e \bar{\nu}_e$	17.7 ± 0.4
$\tau \rightarrow \nu_\tau \mu \bar{\nu}_\mu$	17.8 ± 0.4
$\tau \rightarrow \nu_\tau \pi^-$	10.8 ± 0.6
$\tau \rightarrow \nu_\tau \pi^- \pi^0$	22.6 ± 1.1

Table 5: Branching ratios for the largest three-prong channels. [8]

decay	BR (%)
$\tau \rightarrow \nu_\tau \pi^- \pi^+ \pi^-$	6.4 ± 0.4
$\tau \rightarrow \nu_\tau \pi^- \pi^+ \pi^- \pi^0$	4.9 ± 0.6

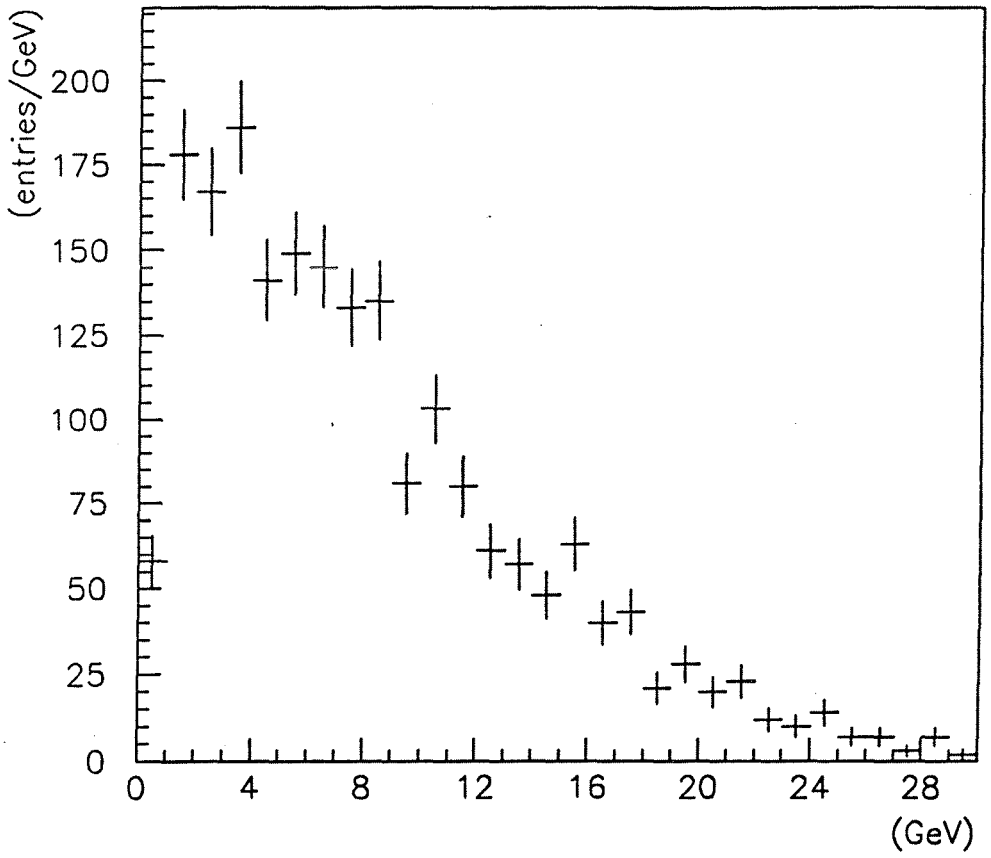

Figure 7: P_T -distribution of the charged tracks seen in three-prong tau decays.

4 Event Selection

In order to get a reliable result, we need a clean and large sample of three-prong tau events. These requirements can quite easily be met in DELPHI because of the high statistics and the precision tracking.

The event sample was extracted from 300 000 Z^0 events applying the following cuts [9]:

1. Only charged particles with momentum greater than 0.5 GeV were kept;

2. the background from hadronic events was minimised by demanding a maximum of six charged tracks, one of which had to be isolated in angle from all the other particles in the event by at least 155°;

3. contamination from $\gamma\gamma$-events was minimized by requiring that the total visible energy in the event be greater than 8 GeV and that the transverse missing momentum $\vec{P}_{Tmiss}$ be greater than 0.4 GeV. $\vec{P}_{Tmiss}$ is defined as the vector sum of the momenta transverse to the beam direction;

4. in order to reduce the background coming from $e^+e^- \rightarrow e^+e^-$ events the total electromagnetic energy in the event had to be smaller than 70 GeV;

5. contamination from $e^+e^- \rightarrow \mu^+\mu^-$ events was removed by requiring the total visible momentum to be less than 75 GeV.

These cuts reduce the initial sample to about 3000 $Z^0 \rightarrow \tau^+\tau^-$ candidates. In the final selection cuts on the track quality was applied, requiring especially that the tracks forming the three-prong have sufficient information from the VD. For simplicity, only events with exactly four tracks were accepted.

Cuts on the three-prong tracks:

1. The tracks must be well inside all layers of the VD, implying that θ

1. The tracks must be well inside all layers of the VD, implying that θ should be between 45°and 135°.

2. at least two hits in the VD. If exactly two hits, they must not be in the overlaps of the same layer since this would give a bad refit of the track.

This leaves 683 events which were used in the subsequent analysis.

5 Errors on Vertices

5.1 Method

5.1.1 Track approximations and track fits

In a homogenous magnetic field, the track of a charged particle has the form of a helix. With the field parallel to the z-direction, the particle will then trace out a circle in the $r\phi$-plane. In a projection perpendicular to the beam the tracks can therefore be approximated with circle-arcs.

In a projection parallel to the beam, the tracks are sinusiodal. However, because of the large momentum carried by the tracks, their form will be close to a straight line, at least over a distance that is much smaller than the radius of curvature of the track.

The data recorded in an event is processed through a track finding algorithm and fits are made to the found tracks. In this first track fit, the information from the VD is not taken into account. However, the track fit can be substantially improved by refitting the tracks using this information.

The refitting can be done in several ways. Here the tracks were refitted using two different methods. The first one (the Kalman filter method [10] [11]) makes a refit using both the old track fit and the VD hits. It takes multiple scattering into account. The second method (the circle method [12]) fits a circle through the VD hits, the radius of the circle being known through the momentum and the magnetic field.

5.1.2 Calculation of the error

The error in the $r\phi$-plane on a vertex can be estimated by calculating the crossing point of two tracks and measuring the shortest distance to the third track. This impact parameter is called I_{rmiss}.

Since the measured distance is approximately perpendicular to the direction of flight of the initial particle, this method measures the error only in that direction. It is worth noting that the error is much larger parallel to the direction of flight. The reason is that the opening angles between the tracks are small. A relatively small error in the track position will then translate into a large error in the longitudinal vertex position, see figure 8.

The longitudinal error can be calculated if we know the initial direction of flight. This direction can suitably be approximated with the thrust axis for the three particle tracks. Here we will only give a very rough approximation and set the initial particle direction equal to the direction of one of the tracks. from figure 8 we then get

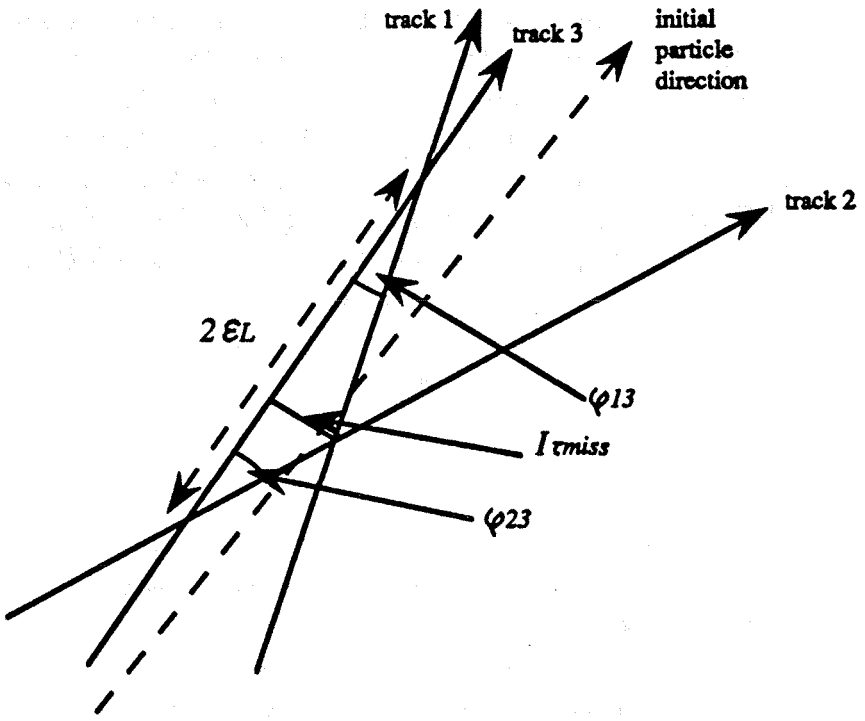

Figure 8: Approximation of the longitudinal error ϵ_L. (The tracks are approximated with straight lines.)

$$\epsilon_L \approx \frac{1}{2} I_{rmiss} \left(\frac{1}{\tan \phi_{13}} + \frac{1}{\tan \phi_{23}} \right). \quad (1)$$

I_{rmiss} is calculated as follows: the tracks are refitted using the information from the VD. The two points of intersection between two tracks of opposite charge are calculated approximating the tracks with circles in $r\phi$. The distances from these two points to the third track are calculated. I_{rmiss} is then chosen as the smallest of these two distances, see figure 9.

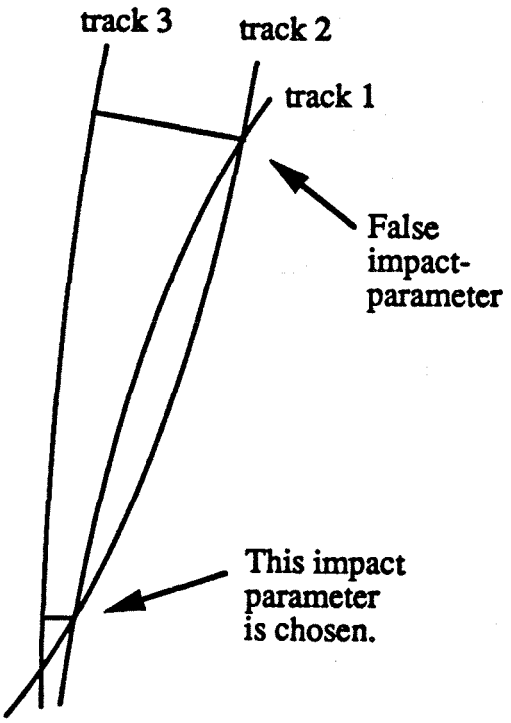

Figure 9: Calculation of I_{rmiss}.

Recall that the error parallel to the tau flight direction is big, typically of the same order as the tau flight distance itself (a couple of millimeters). Therefore it is not a useful approach to determine I_{rmiss} by choosing the vertex which is on the physically correct side of the beamspot.

I_{rmiss} is calculated for every pair of oppositely charged tracks. The sign of I_{rmiss} is determined according to the geometrical sign convention; negative if the vertex is within the circle of the third track and positive if the vertex is outside.

The vertex error in the z-direction is called I_z. Calculating I_z, the tracks are approximated with straight lines. A z-coordinate for each track is calculated by inserting the transverse coordinates for the vertex in the straight line equations for the three tracks. The differences between these z-coordinates, $z_i - z_j$, (where $i, j = 1, 2, 3$ and $i \neq j$) is identified with I_z. This method gives three I_z per event.

5.2 Results

5.2.1 Resolution in the $r\phi$-plane

Refitting the tracks with the Kalman filter method, we get the I_{rmiss} distribution shown in figure 10. The circle method results in the I_{rmiss} distribution in figure 11. We see that the circle method in fact gives a slightly better result. The most important improvement is the significant reduction of the tails. The results presented below are therefore based on the circle method. None of the distributions (figure 10 and 11) is well fit by a Gaussian.

Equation (1) can be used to find the order of magnitude of the longitudinal error. Using $\sigma_{rmiss} = 56$ μm and $\phi_{13} = \phi_{23} = 3°$ we get $\sigma_L \approx 1$ mm.

5.2.2 Resolution in the z-direction

The measurement of I_z gave the result shown in figure 12. Neither is this distribution well fit by a Gaussian.

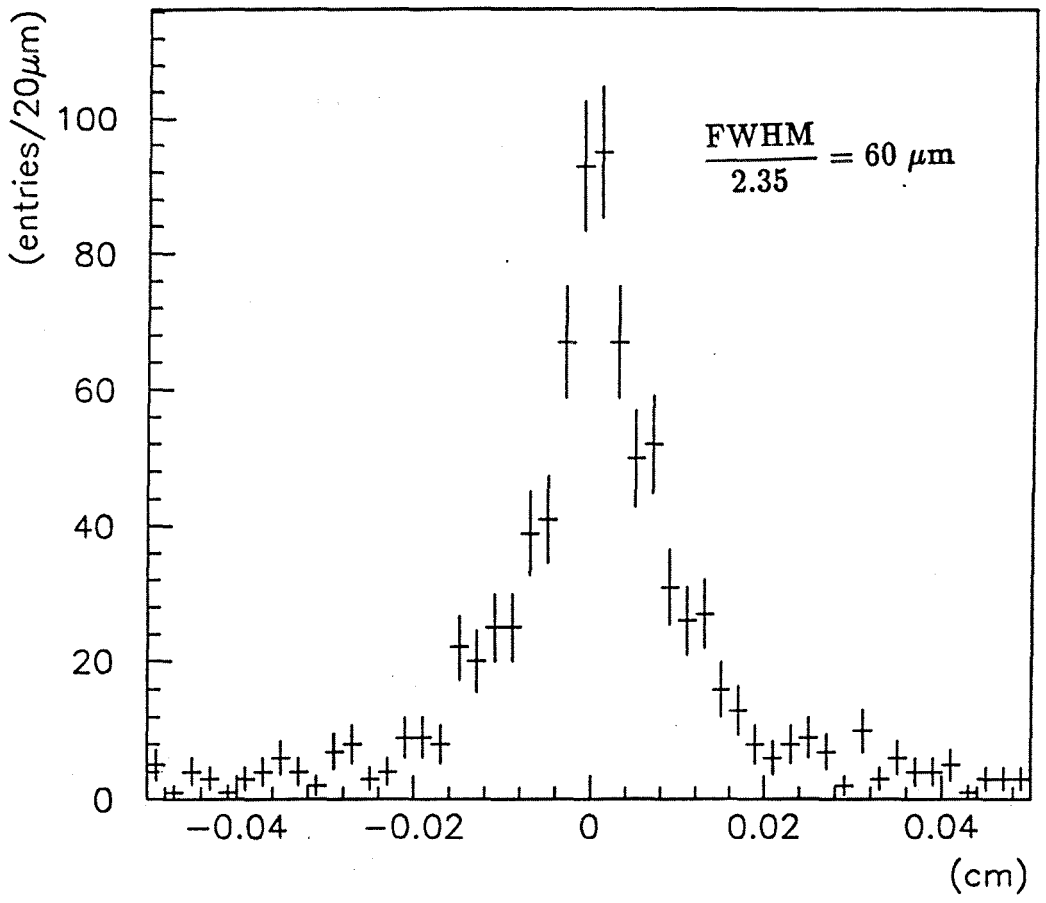

Figure 10: $I_{\tau miss}$**-distribution with the Kalman filter method.**

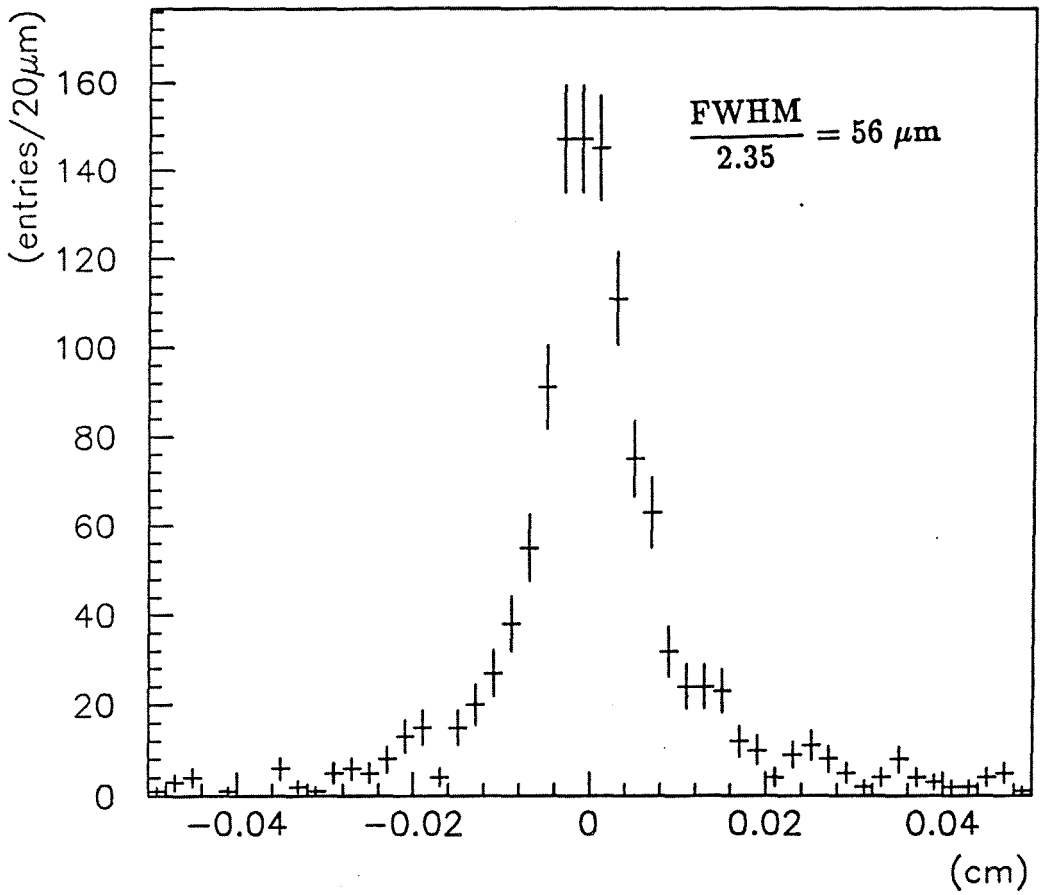

Figure 11: I_{rmiss}-distribution using the circle method.

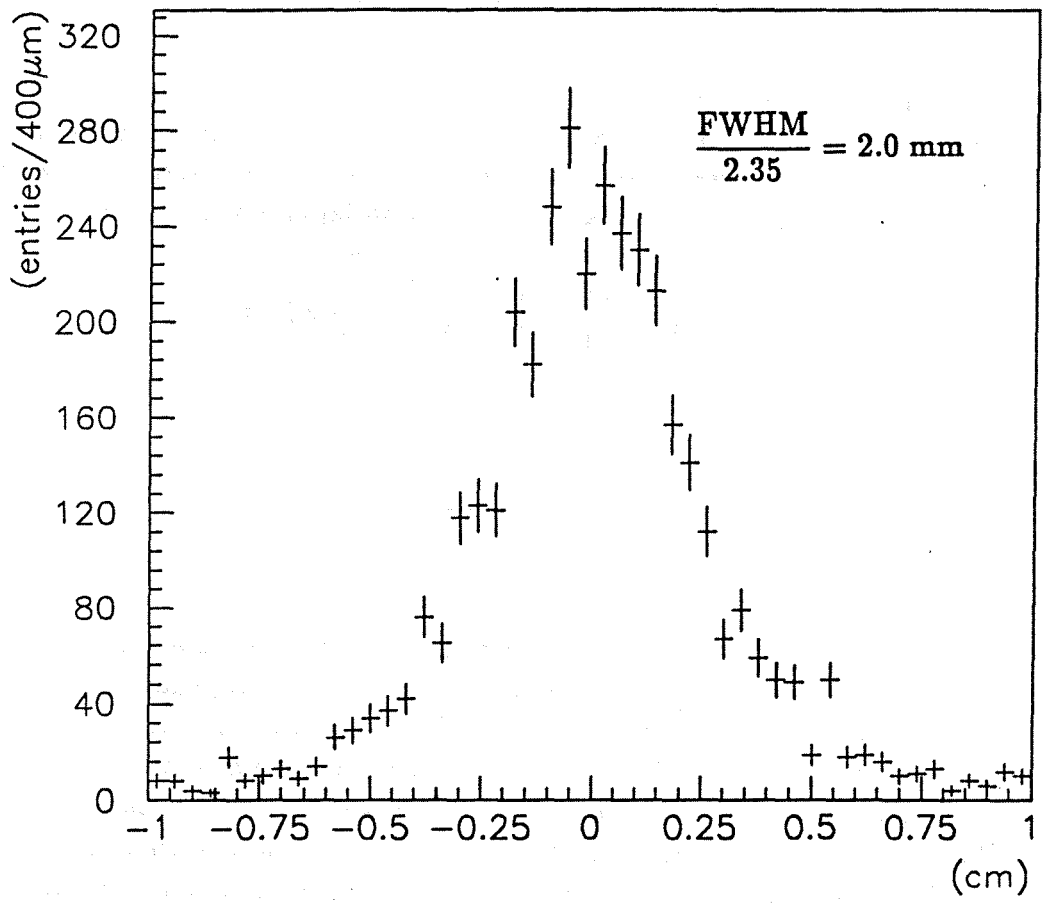

Figure 12: I_x-distribution.

6 Errors on Tracks

The vertex error distribution obtained in the previous section can be used to estimate the track errors[1]. To do this we need to express $I_{\tau miss}$ as a function of the track errors. Since $I_{\tau miss}$ is small compared to the radius of curvature of the tracks, we can approximate the tracks with straight lines. The vertex is constructed from track 1 and track 2, and the errors on the angles ϕ_i and on the transverse momentum P_T are neglected. This gives the error propagation formula

$$I_{\tau miss} = \frac{\sin\phi_{23}}{\sin\phi_{12}}\epsilon_1 + \frac{\sin\phi_{31}}{\sin\phi_{12}}\epsilon_2 + \epsilon_3 \tag{2}$$

where the indices i,j denote the track number. ϕ_{ij} is the opening angle between track i and j counted from track i, and ϵ_i is the error on track i at the tau decay vertex. The derivation of equation (2) is referred to appendix A. Assuming that the three track errors ϵ_i are independent, we get

$$\sigma_{\tau miss} = \sqrt{\left(\frac{\sin\phi_{23}}{\sin\phi_{12}}\sigma_1\right)^2 + \left(\frac{\sin\phi_{31}}{\sin\phi_{12}}\sigma_2\right)^2 + \sigma_3^2} \tag{3}$$

where the standard deviation of the track error, σ_i, can be expressed as

$$\sigma_i = \sqrt{\left(\frac{\sigma_{ms}}{P_{T_i}}\right)^2 + \sigma_{al}^2}.$$

Here σ_{ms}/P_{T_i} is the error in track i due to multiple scattering and σ_{al} is the error caused by alignment errors and the finite intrinsic resolution. There are also errors arising from the uncertainty in momentum and the energy loss in the beam tube and the detector, but these will be neglected here, since they give a much smaller contribution than the two sources mentioned above.

The assumption that σ_{ms} and σ_{al} are mere constants is an oversimplification. They both depend on the geometry of the track; how many hits that were used in the refitting of the track and the relative positions of these hits. In addition, the multiple scattering has a slight dependence on θ. In the next section these points will be discussed in more detail.

6.1 Theoretical estimation of σ_{al} and σ_{ms}

The objective of this section is to find the approximative magnitudes of the errors from multiple scattering and alignment. In a detailed calculation one

[1] 'track error' is short for 'error on the impact parameter at perigee for a track'.

would have to take into account the number and location of the hits for every track and its position in θ as well as the relative occurences of the possible hit combinations. We will not do this. Instead, results from separate calculations for every possible hit combination for two different angles is presented.

6.1.1 Alignment and resolution effects

The error on the impact parameter depends partially on the hit error combined with the geometry of the track; how many hits that are used in the fit and in which layers these hits are located. The hit error in turn depends on the intrinsic resolution in the detector and the alignment error. For short, this error is here referred to as the alignment error.

The distribution of the error in the hit position on a plaquette is shown in figure 13. We see that it is reasonable to set $\sigma_{hit} \approx 10$ μm.

According to appendix B and [13], we have for two hits

$$\sigma_{al} = \sqrt{\left(1 + \frac{R_1}{R_2 - R_1}\right)^2 \sigma_{hit1}^2 + \left(\frac{R_1}{R_2 - R_1}\right)^2 \sigma_{hit2}^2} \; .$$

and for hits in all three layers the error is given by

$$\sigma_{al} = \sqrt{\left(\frac{R_I + 2R_O}{3(R_O - R_C)}\sigma_C\right)^2 + \left(\frac{1}{3}\sigma_I\right)^2 + \left(\frac{R_I + 2R_C}{3(R_O - R_C)}\sigma_O\right)^2} .$$

6.1.2 Results

The numerical results obtained from the formulas above are given in table 6.

Table 6: σ_{al} for different hit combinations. (CI = hits in the closer and inner layers, CO = hits in the closer and outer layers etc.)

hits in	σ_{al} (μm)
CI	44
CO	27
IO	66
CIO	27

6.1.3 Multiple scattering

When an electrically charged particle traverses a layer of matter, it is deflected from its path because of elastic scattering off the electrons and nuclei

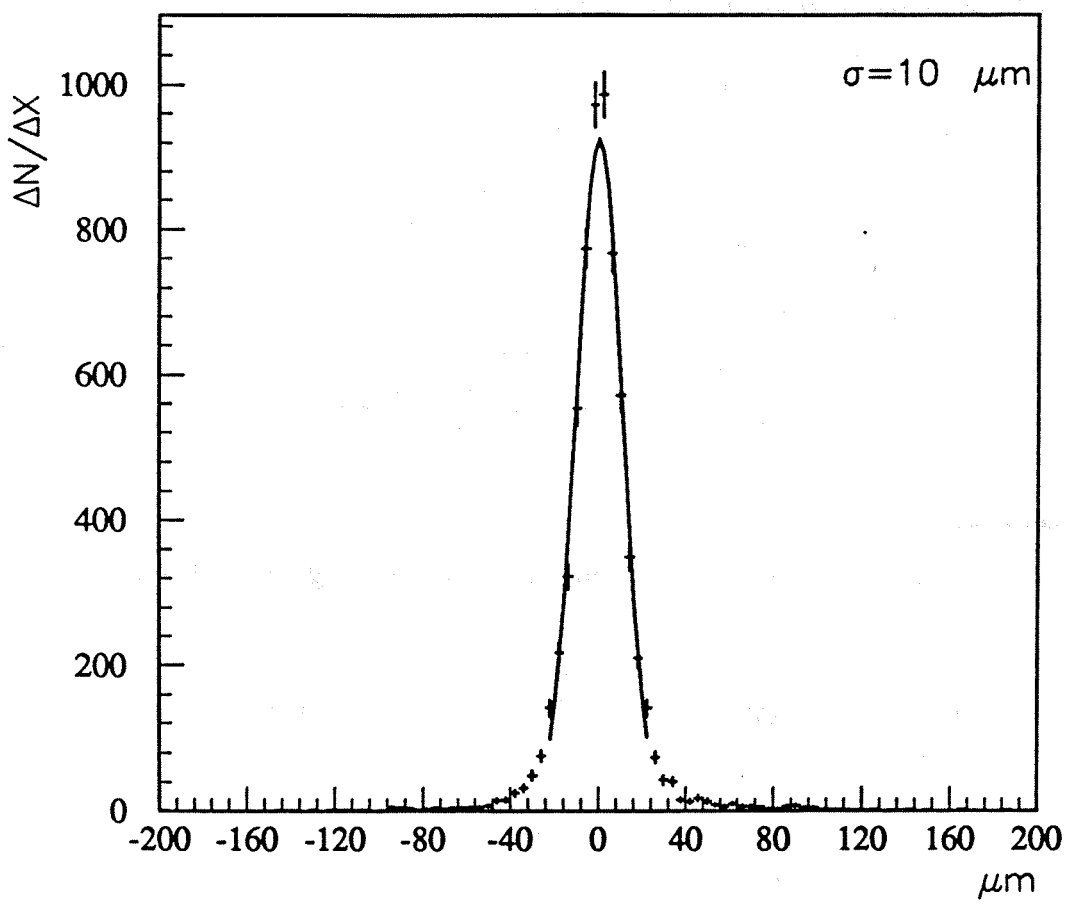

Figure 13: Hit error distribution. [7]

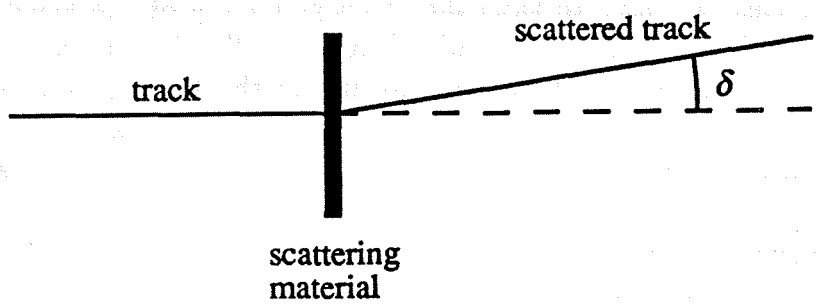

Figure 14: Definition of the deviation angle δ due to multiple scattering.

multiple scattering causes a random deviation δ from the original particle trajectory, see figure 14.

An approximate value of the standard deviation of δ is given by *Molières formula* (see [10] for instance)

$$\sigma_\delta = \frac{14.1\text{MeV}}{\beta cp} z \sqrt{\frac{x}{X_0}} \left(1 + 0.038 \ln \frac{x}{X_0}\right)$$

where βc is the velocity of the particle, z is the absolute value of the charge number, X_0 the radiation length of the material and x the traversed thickness. The derivation starts from the Rutherford formula for scattering of point-like spinless particles. We are here only interested in the projection of δ in the $r\phi$-plane, $\delta^{r\phi}$. Setting $\beta \approx 1$ and $z = 1$ gives

$$\sigma_\delta^{r\phi} = \frac{14.1\text{MeV/c}}{P_T} \sqrt{\frac{t}{X_0 \sin\theta}} \left(1 + 0.038 \ln \frac{t}{X_0 \sin\theta}\right) \qquad (4)$$

where t is the thickness of the scattering layer. This formula describes the multiple scattering in a thin layer as a function of P_T. Setting $\theta = 90°$ gives $\sigma_\delta^{r\phi} \approx 0.60$ mrad for the silicon pads and $\sigma_\delta^{r\phi} \approx 0.70$ mrad for the beampipe. $\theta = 45°$ gives respectively 0.73 mrad and 0.85 mrad.

On its way out from the production point, a particle is first scattered an angle δ_B by the beampipe, *then* the first measurement of the track position is obtained in the closer layer of the VD. At the same time the particle is scattered again (with angle δ_C). As it reaches the outer layer it has already

been scattered in three thin layers, not considering the overlaps. In the track reconstruction, the original track is finally identified with the best fit to the hits obtained.

In order to calculate the error on the impact parameter that this procedure causes, we have to take the exact geometry of the event into account. The formulas (12) and (14) derived in appendix B and used in the previous section are useful also here, but instead of the hit errors we put in the errors caused by multiple scattering. The sum in quadrature is taken over the scattering angles and not the hit errors, which are now correlated.

Consider figure 15. The horisontal line is the initial track direction. The deviations ϵ from this direction can be expressed in terms of the scattering angles δ_B, δ_C and δ_I. Using the assumptions that the tracks are approxi-

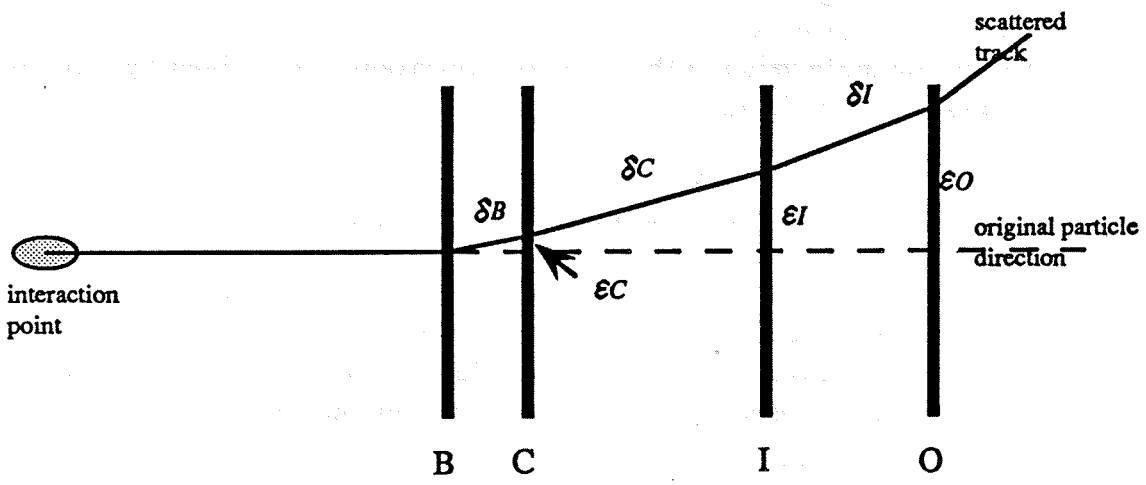

Figure 15: Calculation of the contribution from multiple scattering to the impact parameter error.

mately perpendicular to the plaquettes and that the scattering angles are very small we find that the errors on each layer can be written as

$$\begin{aligned} \epsilon_C &= \delta_B(R_C - R_B) \\ \epsilon_I &= \delta_B(R_I - R_B) + \delta_C(R_I - R_C) \\ \epsilon_O &= \delta_B(R_O - R_B) + \delta_C(R_O - R_C) + \delta_I(R_O - R_I). \end{aligned}$$

6.1.4 Results

Using the above expressions in equations (12) and (14), rearranging and summing in quadrature over independent terms gives the results quoted in table 7.

Table 7: σ_{ms} in μmGeV/c for different hit combinations.

hits in	$\theta = 45°$	$\theta = 90°$
CI	123	101
CO	107	88
IO	449	370
CIO	67	55

6.2 Experimental estimation of σ_{al} and σ_{ms}

$I_{\tau miss}$ depends on the track errors ϵ_i and the relative orientation of the tracks. Thus we should be able to determine σ_{ms} and σ_{al} by comparing the measured $I_{\tau miss}$ with $\sigma_{\tau miss}$ calculated from equation (3) for every event and choosing the values σ_{al} and σ_{ms} that give the best agreement. This might be done by minimizing

$$Q(\sigma_{al}, \sigma_{ms}) = \sum_{k=1}^{N} \left((\frac{I_{\tau miss,k}}{\sigma_{\tau miss,k}})^2 - 1 \right)^2 \qquad (5)$$

with respect to σ_{al} and σ_{ms}, where N is the number of measured $I_{\tau miss}$. Equation (5) can be understood by considering a stochastic variable X with variance $V(X) = \sigma^2$ and mean $E(X) = m$. The variance can also be written

$$\sigma^2 = V(X) = E(X^2) - (E(X))^2 = E(X^2) - m^2$$

If X has mean $m = 0$ we have

$$\sigma^2 = E(X^2)$$

or

$$1 = E\left((\frac{X}{\sigma})^2 \right).$$

This result implies that the stochastic variable $(\frac{I_{\tau miss}}{\sigma_{\tau miss}})^2$ should have a mean equal to one, which explains the form of equation (5).

However, using equation (5) as it stands would give very heavy weight to those events where $I_{\tau miss}$ is greater than $\sigma_{\tau miss}$ in comparison with events where they are approximately equal or when $\sigma_{\tau miss}$ is greater than $I_{\tau miss}$. This is undesirable and therefore equation (5) has to be modified. A better weighting of the events is obtained if we instead minimize

$$Q(\sigma_{al}, \sigma_{ms}) = \sum_{k=1}^{N} \left(min\left((\frac{I_{\tau miss;k}}{\sigma_{\tau miss;k}})^2, (\frac{\sigma_{\tau miss;k}}{I_{\tau miss;k}})^2 \right) - 1 \right)^2 . \qquad (6)$$

6.2.1 Results

Minimizing (6) with MINUIT yields

$$\sigma_{ms} = 62 \pm 14 \ \mu\text{mGeV}/c$$

$$\sigma_{al} = 24.4 \pm 2.0 \ \mu\text{m}$$

7 Discussion

The error on secondary vertices is found to be at best 56 μm. This number is valid (approximately) perpendicular to the flight direction. In the longitudinal direction the error is of the same order of magnitude as the flight distances for short lived particles.

The theoretical (tables 6 and 7) and experimental (section 6.2.1) results obtained for the contribution from multiple scattering and alignment errors to the track errors are in reasonable accordance. A comparison of the results for the alignment error (table 6 and the σ_{al}-value in section refsec:expres) suggest that the hit error (figure 13) might be somewhat overestimated.

7.1 Comparison with results obtained using muons

The most straight forward way to measure the error on the impact parameter is to look at muon pair production, $e^+e^- \rightarrow Z^0 \rightarrow \mu^+\mu^-$.

Since both muons come from the same point and are nearly back to back we can express $I_{\mu miss}$ as the sum of the individual track errors:

$$I_{\mu miss} = \epsilon_{track1} + \epsilon_{track2} \tag{7}$$

This gives directly the error on the impact parameter if we assume that the errors from the two tracks are equal and independent, i e can be added in quadrature, in which case we get

$$\sigma_{track} = \frac{\sigma_{\mu miss}}{\sqrt{2}}. \tag{8}$$

In DELPHI the current value on $\sigma_{\mu miss}$ is 34 μm in $r\phi$, see figure 16. This gives, using equation (8), an impact parameter error on high P_T tracks of 24 μm in $r\phi$.

Because of the high P_T of muon tracks, $I_{\mu miss}$ will be quite insensitive to multiple scattering. Thus we can in this case neglect the first term in (4) and set $\sigma_{al} \approx 24$ μm, which agrees well with the previously obtained results.

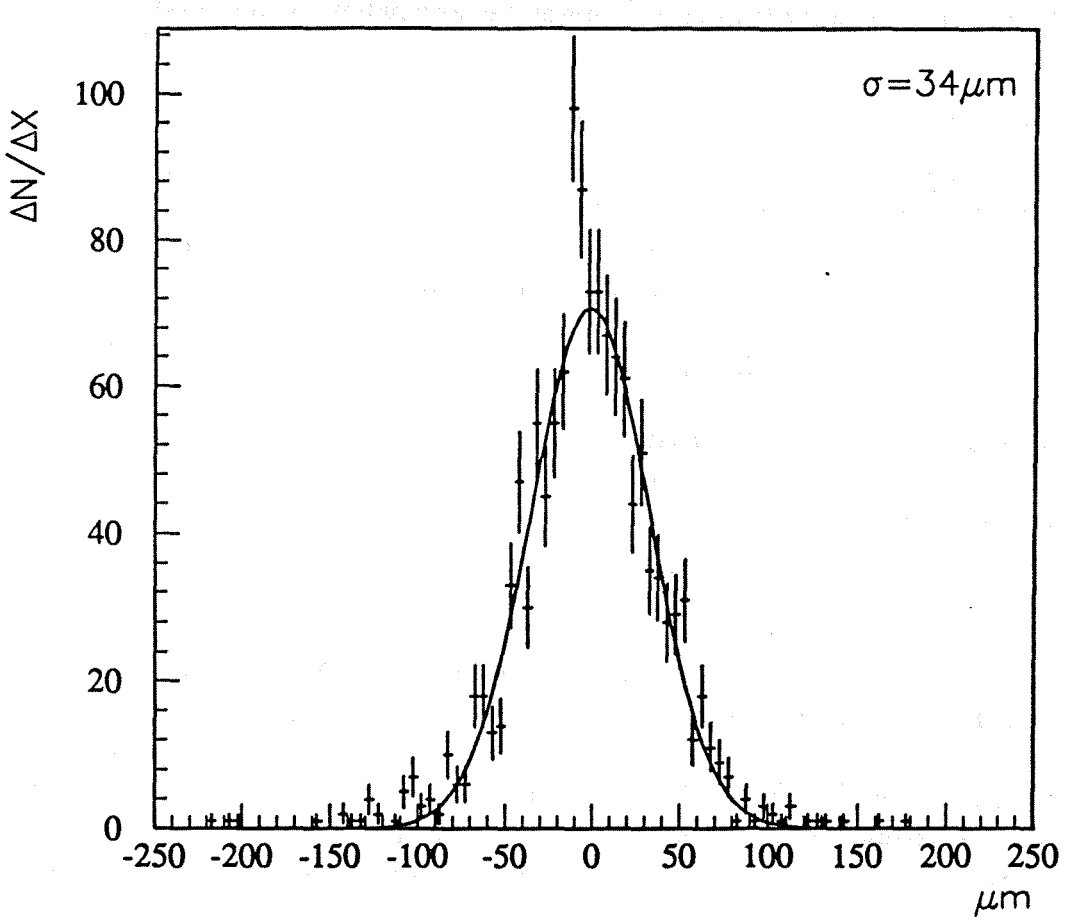

Figure 16: Muon miss distance $I_{\mu miss}$. [7]

8 Acknowledgements

It is a pleasure for me to express my gratitude to all of those who have helped me during these months.

First of all I would like to thank my supervisor Tord Ekelöf for his support and guidance during the course of this study and for giving me the opportunity to work with the DELPHI collaboration, a very stimulating environment. I sincerely thank Gunnar Mæhlum who spent so much of his valuable time helping me with everything from practical details such as finding a nice office to carefully explaining the software structure or the subtilities of the detector and for his persistance in trying to improve my free style swimming.

In addition I would like to express my deep appreciation of all the members of the micro-vertex subgroup for many stimulating and helpful discussions and of everyone who has contributed to the completion of this report.

A Derivation of the $I_{\tau miss}$ Error Propagation Formula

We want to know how errors in the track positions affect the value of $I_{\tau miss}$, which is itself an error; if the tracks have *no* errors, $I_{\tau miss}$ will of course be zero.

$I_{\tau miss}$ does not depend on the track parameters ϕ_i and t_i but only on their errors $d\phi_i$ and dt_i. In fact, $I_{\tau miss}$ is equivalent to the error dL on the distance L defined in figure 17. L is the distance of closest approach for three tracks in two dimensions. In the tau decay, we know that L is always zero, but this subcondition does of course not affect the form of the error propagation formula.

The tracks are approximated with straight lines and expressed using the coordinates illustrated in figure 18.

$$
\begin{aligned}
y_1 &= x_1 \tan\phi_1 - t_1/\cos\phi_1 \\
y_2 &= x_2 \tan\phi_2 - t_2/\cos\phi_2 \\
y_3 &= x_3 \tan\phi_3 - t_3/\cos\phi_3
\end{aligned}
$$

The subscripts 1, 2 and 3 denote the track number.

According to figure 17, L is the difference between the points (x_m, y_m) and (x_v, y_v) where (x_v, y_v) is the crossing point of tracks 1 and 2, and (x_m, y_m) is the point on the third track that is closest to (x_v, y_v):

$$L = \sqrt{(x_m - x_v)^2 + (y_m - y_v)^2}. \tag{9}$$

The crossing point of tracks 1 and 2 is

$$x_v = \frac{t_1/\cos\phi_1 - t_2/\cos\phi_2}{\tan\phi_1 - \tan\phi_2}$$

$$y_v = x_v \tan\phi_1 - t_1/\cos\phi_1$$

The point (x_m, y_m) is found by minimizing

$$\sqrt{(x_3 - x_v)^2 + (y_3 - y_v)^2}$$

with respect to x_3 and y_3. We find the minimum at

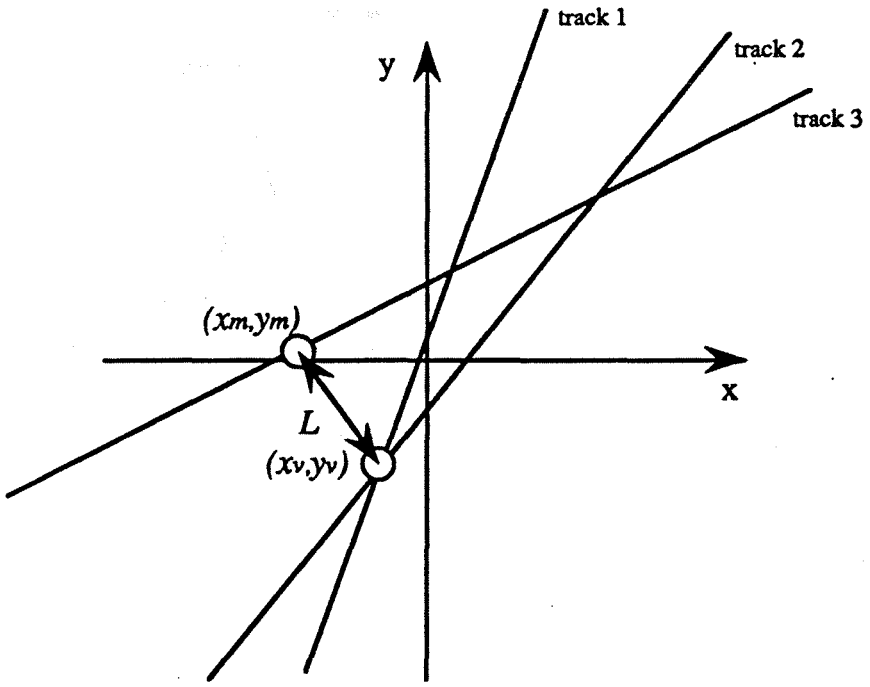

Figure 17: Definition of L and the points (x_m, y_m) and (x_v, y_v).

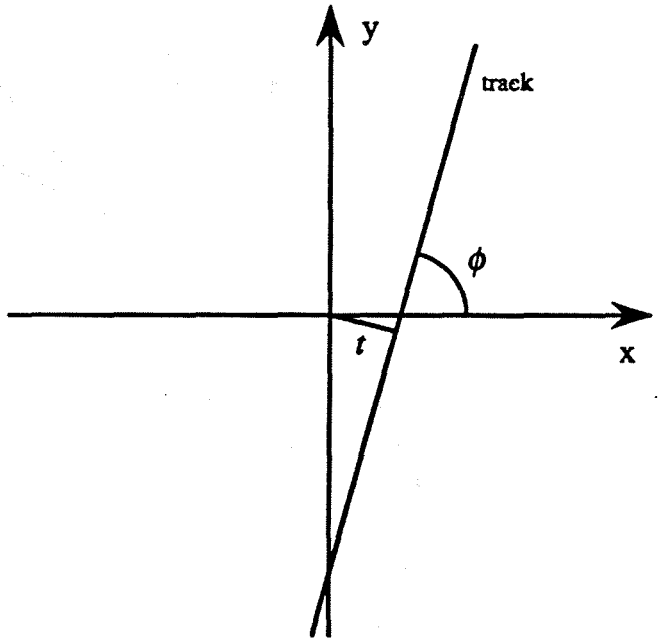

Figure 18: Definition of the coordinates ϕ and t.

$$x_m = \frac{x_v - t_3 \tan\phi_3/\cos\phi_3 + \tan\phi_3(x_v \tan\phi_1 - t_1/\cos\phi_1)}{1 + \tan^2\phi_3}$$

$$y_m = x_m \tan\phi_3 - t_3/\cos\phi_3.$$

Logarithmic differentiation of equation (9) gives the error propagation formula

$$dL = \frac{1}{L^2}\sum_{i=1}^{3}\left((x_m - x_v)(\frac{\partial x_m}{\partial t_i} - \frac{\partial x_v}{\partial t_i}) + (y_m - y_v)(\frac{\partial y_m}{\partial t_i} - \frac{\partial y_v}{\partial t_i})\right) dt_i \quad (10)$$

Note that the angle errors $d\phi_i$ are neglected in this formula. Only the transverse deviations dt_i of the tracks (at perigee) are considered. Putting the explicit expressions for x_m, y_m, x_v and y_v into equation (10) gives, after a short calculation,

$$I_{rmiss} = dL = \frac{\sin\phi_{23}}{\sin\phi_{12}}dt_1 + \frac{\sin\phi_{31}}{\sin\phi_{12}}dt_2 + dt_3 \quad (11)$$

where ϕ_{ij} is, as before, short for $\phi_i - \phi_j$. Formula (11) is the same as formula (2) except for a slight difference in notation: dt_i corresponds to ϵ_i.

B Derivation of the Impact Parameter Error Formulas

A straight line approximation is used. Note that the final expressions obtained here require that the hit errors be independent.

B.1 Two hits

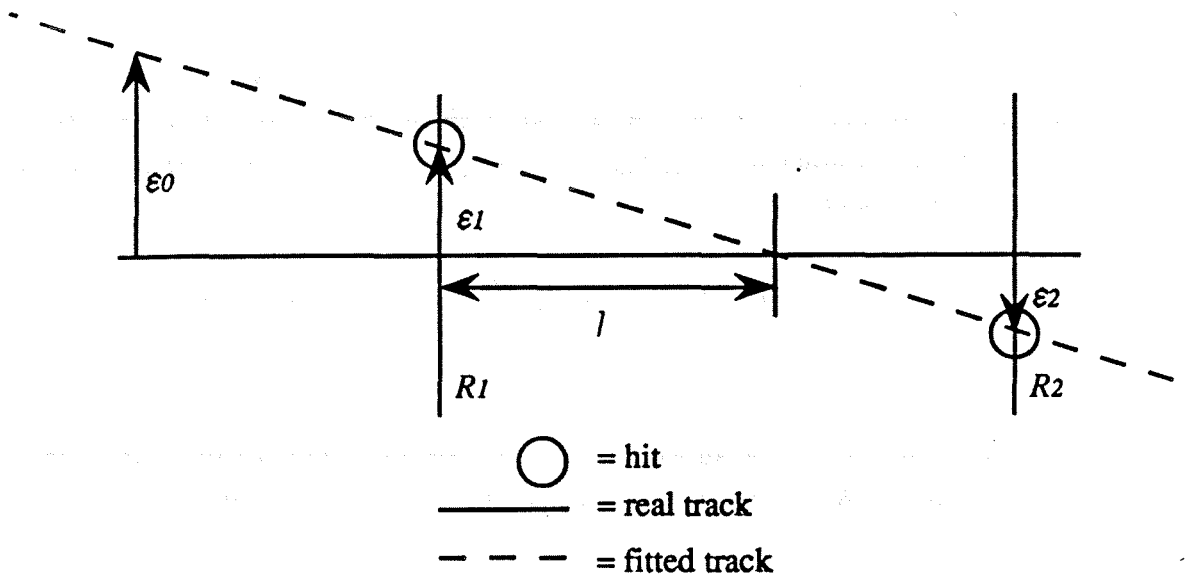

Figure 19: The errors ϵ_1 and ϵ_2 produce the error ϵ_0.

The geometry is illustrated in figure 19: the horisontal line is the trajectory the particle would have had if no multiple scattering had occurred. The dashed line is the fitted track. It goes through the two hits, shown as two crosses in the figure.

The hit errors are denoted with ϵ_1 and ϵ_2. They give rise to the error ϵ_0 at perigee. $R_1 + l$ is the crossing point of the fitted track and the true track. For

simplicity, the same notation has been used for the stochastic variables (wich have properties like variances and means) and the corresponding random values (which are mere numbers).

Using the law of conform triangles we immediately get

$$\frac{\epsilon_0}{\epsilon_1} = \frac{R_1 + l}{l}$$

and

$$\frac{\epsilon_1}{\epsilon_2} = \frac{l}{R_2 - R_1 - l}$$

which gives

$$\epsilon_0 = \left(1 + \frac{R_1}{R_2 - R_1}\right)\epsilon_1 + \frac{R_1}{R_2 - R_1}\epsilon_2 \qquad (12)$$

The expression $(R_1)/(R_2 - R_1)$ is called the leverarm.

If the errors ϵ_1 and ϵ_2 are independent, we can add the terms in equation (12) in quadrature. Denoting the standard deviation of ϵ_i with σ_i we then arrive at the final expression

$$\sigma_0 = \sqrt{\left(1 + \frac{R_1}{R_2 - R_1}\right)^2 \sigma_1^2 + \left(\frac{R_1}{R_2 - R_1}\right)^2 \sigma_2^2}. \qquad (13)$$

B.2 Three hits

The best straight straight line fit to three points is such that the distance from the middle-point to the line is twice as big as the distance from the two side-points to the line, see figure 20.

The true track is the line $y = 0$. The fitted track is described by the equation

$$y = ax + b$$

where

$$a = \frac{(\epsilon_i - \lambda_i) - (\epsilon_j - \lambda_j)}{R_i - R_j}$$

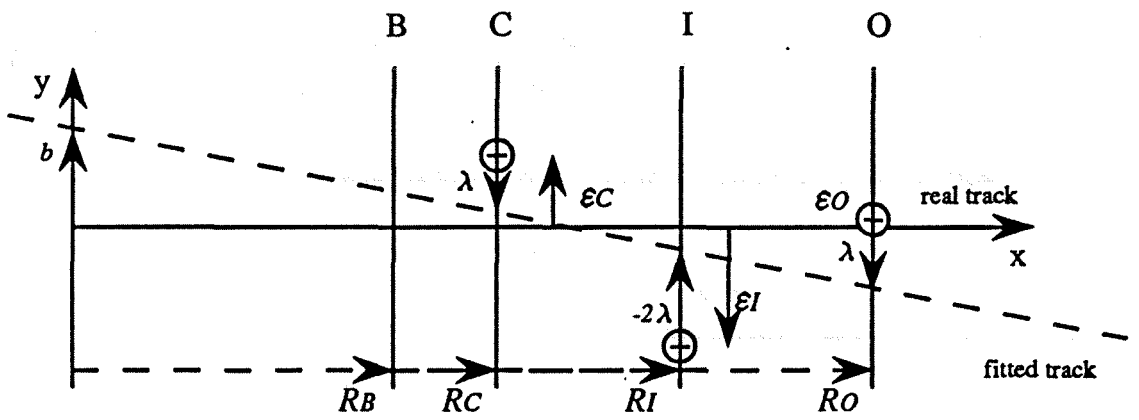

$\lambda_C = \lambda_O = \lambda$

$\lambda_I = -2\lambda$

○ = hit

Figure 20: Impact parameter error for a track with three hits.

$$b = \epsilon_i - \lambda_i - aR_i.$$

The indices i and j refer to the closer, inner and outer layers. We want to calculate b, which is identical to the error on the impact parameter. Eliminating λ and solving for b gives

$$b = \frac{R_I + 2R_O}{3(R_O - R_C)}\epsilon_C + \frac{1}{3}\epsilon_I - \frac{R_I + 2R_C}{3(R_O - R_C)}\epsilon_O. \tag{14}$$

If the hit errors ϵ_C, ϵ_I and ϵ_O are independent we can express σ_b as

$$\sigma_b = \sqrt{\left(\frac{R_I + 2R_O}{3(R_O - R_C)}\sigma_C\right)^2 + \left(\frac{1}{3}\sigma_I\right)^2 + \left(\frac{R_I + 2R_C}{3(R_O - R_C)}\sigma_O\right)^2}. \tag{15}$$

References

[1] See for instance D. H. Perkins, Introduction to High Energy Physics, Addison-Wesley Publishing Company, Inc. (1987).

[2] G. Altarelli et al., Z^0 Physics at LEP, CERN 89-08 (1989).

[3] P. Allport et al., Physics aspects of the DELPHI Vertex detector, CERN-EP/88-82.

[4] DELPHI Collaboration, The DELPHI detector at LEP, Nuclear Instruments and Methods A303 (1991) 233.

[5] G. Anzivino et al., The DELPHI Silicon Strip Micro-Vertex Detector, Nuclear Instruments and Methods in Physics Research A263 (1988) 215.

[6] E. Belau et al., Charge Collection in Silicon Strip Detectors, Nuclear Instruments and Methods 214 (1983) 253.

[7] G. Maehlum, The DELPHI Silicon Microstrip Vertex Detector, PhD Thesis (under preparation), (1992).

[8] C Kiesling, τ Physics, High Energy Electron-Positron Physics edited by A. Ali and P. Söding (1988).

[9] DELPHI Collaboration, Determination of Z^0 Resonance Parameters and Couplings from its Hadronic and Leptonic Decays, CERN–PPE/91–95, submitted to Nuclear Physics B, (1991).

[10] R. K. Bock et al., Data Analysis Techniques in High Energy Physics Experiments, Cambridge University Press (1990).

[11] P. Billoir, FKRFIT, DELPHI program library.

[12] V. Chabaud, FT2DTK, DELPHI program library.

[13] Micro-vertex group, DELPHI Micro-vertex Detector, Addendum to Technical Proposal, DELPHI 86-86 GEN-52.